RSC Advances

PAPER

View Article Online
View Journal | View Issue

Cite this: *RSC Adv.*, 2021, **11**, 24398

Modulation of electrophoresis, electroosmosis and diffusion for electrical transport of proteins through a solid-state nanopore†

Jugal Saharia,[a] Y. M. Nuwan D. Y. Bandara, ‡[a] Buddini I. Karawdeniya, §[a] Cassandra Hammond,[a] George Alexandrakis[b] and Min Jun Kim *[a]

Received 19th May 2021
Accepted 3rd July 2021

DOI: 10.1039/d1ra03903b

rsc.li/rsc-advances

Nanopore probing of molecular level transport of proteins is strongly influenced by electrolyte type, concentration, and solution pH. As a result, electrolyte chemistry and applied voltage are critical for protein transport and impact, for example, capture rate (C_R), transport mechanism (*i.e.*, electrophoresis, electroosmosis or diffusion), and 3D conformation (*e.g.*, chaotropic *vs.* kosmotropic effects). In this study, we explored these using 0.5–4 M LiCl and KCl electrolytes with holo-human serum transferrin (hSTf) protein as the model protein in both low (±50 mV) and high (±400 mV) electric field regimes. Unlike in KCl, where events were purely electrophoretic, the transport in LiCl transitioned from electrophoretic to electroosmotic with decreasing salt concentration while intermediate concentrations (*i.e.*, 2 M and 2.5 M) were influenced by diffusion. Segregating diffusion-limited capture rate (R_{diff}) into electrophoretic ($R_{diff,EP}$) and electroosmotic ($R_{diff,EO}$) components provided an approach to calculate the zeta-potential of hSTf (ζ_{hSTf}) with the aid of C_R and zeta potential of the nanopore surface (ζ_{pore}) with (ζ_{pore}–ζ_{hSTf}) governing the transport mechanism. Scrutinization of the conventional excluded volume model revealed its shortcomings in capturing surface contributions and a new model was then developed to fit the translocation characteristics of proteins.

Introduction

Nanopores are nanofluidic apertures spanning an impervious membrane that separates two electrolyte reservoirs. When an appropriate voltage bias is applied across the membrane, a molecule translocates from one chamber (*cis*) to the other (*trans*), perturbing the open pore current and generating resistive pulses that are characteristic of the molecule under analysis. The applications of nanopores span a wide range of fields such as genomics,[1,2] proteomics,[3–6] glycomics,[7,8] virology,[9–11] and lipid nanoparticles.[12–14] Analyte transport generally occurs through electrophoresis, electroosmosis, dielectrophoresis or diffusion mechanisms.[15–18] Nanopore and analyte surface charges play an integral role in electrophoresis and electroosmosis driven transport.[19–22] Depending on the surface charge of the nanopore and the analyte, electrophoretic and electroosmotic forces (F_{EP} and F_{EO} respectively) can be opposing or reinforcing. Electrophoresis is mainly dictated by the analyte charge (pH-dependent) and applied voltage whereas electroosmosis primarily relies on the nanopore surface charge (pH-dependent), electrolyte concentration and applied voltage. The nanopore surface charge is a complex interfacial property due to the nanopore's restricted volume and depends on a host of factors such as pH,[23] surface head groups,[24,25] and fabrication method.[26,27] For charge-neutral molecules, electroosmosis is imperative for translocations to occur.[8,28] Moreover, it has been shown that in case of charged particles, electroosmosis can capture particles against electrophoresis, the key factors being the nanopore surface (for electroosmosis) and particle charge (for electrophoresis) which are dependent on the solution pH.[16,18] The electrolyte concentration also plays a vital role in the electroosmotic transport mechanism.[29,30] For example, at higher electrolyte concentrations, the electrical double layer (EDL) which has been established to come to the fore in the electroosmosis-dominant transport mechanism, would be more compact and *vice versa* at lower concentrations. The activation of surface charge effects by electrolyte tuning is also evident by the deviation of the expected open-pore conductance from the observed values at low electrolyte concentrations if surface contributions are not accounted for properly.[31,32] Thus, by tuning the electrolyte concentration, one can tune the magnitude of the contribution of EO to the overall transport and thereby, the capture rate (C_R) and direction/magnitude of

[a]*Department of Mechanical Engineering, Southern Methodist University, Dallas, TX 75275, USA. E-mail: mjkim@lyle.smu.edu*

[b]*Department of Bioengineering, University of Texas at Arlington, Arlington, TX 76019, USA*

† Electronic supplementary information (ESI) available. See DOI: 10.1039/d1ra03903b

‡ Y. M. N. D. Y. B is presently employed at University of California, Riverside.

§ B. I. K is presently employed at The Australian National University.

molecular transport depending on whether F_{EO} opposes or reinforces the F_{EP} and their relative magnitudes. Electroosmosis can be minimized through nanopore surface modifications where the surface remains charge-neutral over a range of pH values.[24] In our previous work, we have shown that a simple change to the electrolyte chemistry during pore fabrication (using controlled dielectric breakdown, CDB) yields nanopores with considerably different surface chemistry compared to the conventional CDB nanopores. The surface charge density of these chemically tuned CDB (CT-CDB) nanopores do not change appreciably up to pH ~8.[27] Since the surface charge of a CT-CDB nanopore at pH ~8 is (slightly) negative, for a negatively charged analyte, if $F_{EP} > F_{EO}$, the translocation would occur under positive voltage polarity and at opposite polarity if $F_{EO} > F_{EP}$.

Electrolytes are known to have a complex effect on the 3D structure of proteins through interactions with, for example, unpaired charged side chains (*e.g.*, crosslinking through multivalent ion binding) and the dipole peptide bonds.[33] Destabilization of the protein occurs if ions bind preferentially to the non-native state over the native state.[34] The electrolyte type, according to the Hofmeister series – originating from the work of Franz Hofmeister nearly 130 years ago – can either have salting-in (chaotropic; destabilizing effects) or salting-out (kosmotropic; stabilizing effects) effects on protein stability.[35] The work of Green *et al.* suggests that the Hofmeister effects are prominent at high salt concentrations (0.5–3 M)[36] – the range where a host of nanopore-based protein profiling experiments are done. More recently, Medda *et al.* showed that these effects are present at physiological concentrations as well.[37] Thus, the electrolyte chemistry plays an important role in both intra- and inter-protein interactions and ultimately on the protein 3D structure.

To test the transport mechanism in response to electrolyte type and concentrations, we used the holo form of hSTf as the model protein. The hSTf is a blood glycoprotein comprised of 679 amino acids, with a molecular weight of ~80 kDa that binds to iron with a high affinity constant (1020 M^{-1}) at physiological pH.[38] This protein is critical for iron homeostasis with iron release from hSTf clefts taking place at lower endosomal pH. In a previous study, we observed hSTf to be dominantly translocating *via* the electrophoretic mechanism at pH ~6 and ~8 while diffusion was seen to play a key role at pH ~4.[3] These observations were inextricably linked with the pI of hSTf (~5.2–5.6), which is also the case with most other nanopore-based protein studies.[19,39] However, that study was done at a relatively high salt concentration (2 M KCl), diminishing the possibility of electroosmosis dominating the transport mechanism due to charge screening. In this study, we used 0.5–4 M LiCl and KCl (mostly in 0.5 M steps, buffered at pH ~ 8) across an appreciably wide voltage range (±50 mV to ±800 mV) to enable the study of C_R, transport mechanism and 3D conformation (*e.g.*, chaotropic *vs.* kosmotropic effects). A shift in responsive voltage polarity correlated to a transition in the transport mechanism from electrophoresis (typically at higher electrolyte concentrations) to electroosmosis through a diffusion phase at intermediate electrolyte concentration levels. Although, in most studies, the applied voltage is chosen arbitrarily to be in high (diffusion-limited) or low (barrier-limited) electric field regime, our results reveal the shortcomings of such choices because C_R was observed to have a voltage threshold where the behavior was considerably different on either side of the said threshold. This is thought to be a combination of voltage driven unfolding coupled with chaotropic/kosmotropic effect of ions in the electrolyte and the magnitude and direction of F_{EP} and F_{EO}. To understand the transport direction, the zeta potential of both the nanopore surface (ζ_{pore}) and holo-hSTf (ζ_{hSTf}) were calculated. Since conventional zeta potential measurements (using a Zetasizer at relatively higher hSTf concentrations) proved to be inadequate, we resorted to measuring the C_R of holo-hSTf as a function of ζ_{pore} to estimate ζ_{hSTf}. Since C_R is dependent on the resultant of competing forces generated by electrophoresis and electroosmosis, when the two forces are equal, the capture rate could be anticipated to approach zero, from which ζ_{hSTf} was calculated.

Methods section

Nanopore fabrication and size estimation

Nanopores were fabricated on nominally ~12 nm thick silicon nitride (Si_xN_y) membranes (NBPX5001Z-HR) purchased from Norcada Inc. using the CT-CDB method[27] with 2 : 9 sodium hypochlorite (425044, Sigma Aldrich): 1 M KCl (P9333, Sigma-Aldrich) buffered at pH ~7 using 10 mM 4-(2-hydroxyethyl)-1-piperazineethanesulfonic acid (HEPES, Sigma-Aldrich, H0527). In brief, an electric field of <1 V nm^{-1} was applied until an abrupt increase in the leakage current was observed which is indicative of a pore formation. After the initial pore-formation, voltage pulses were applied until the pore-size of interest was reached. To measure the final pore size, all content was thoroughly exchanged with 1 M KCl buffered at pH ~7 and a current–voltage (*I–V*) curve was obtained. The diameter of the fabricated pores was calculated using the slope of the *I–V* curve with a formulation that included bulk, surface, and access resistance contributions,

$$G = \left(\frac{1}{G_{bulk} + G_{surface}} + \frac{1}{G_{access}}\right)^{-1} = K\left(\frac{1}{\frac{\pi {r_0}^2}{L} + \frac{\mu|\sigma_p|}{K} \times \frac{2\pi r_0}{L}} + \frac{2}{\alpha \times 2r_0 + \beta \times \frac{\mu|\sigma_p|}{K}}\right)^{-1} \quad (1)$$

where G, r_0, L, K, σ_p, μ, α and β are the open pore conductance, nanopore radius, membrane thickness, electrolyte conductivity, nanopore surface charge density, mobility of counter-ions proximal to the surface and model-dependent parameters (both set to 2).[27,40] Contribution of the access resistance to the overall resistance become significant for pores with low thickness to diameter ratios. For example, this is true for cases where the thickness is comparable or smaller than the pore opening. In our case, the thickness and the pore diameter are comparable and access resistance should be accounted for as shown in eqn (1). We would like to direct the interested readers to ref. 40 for

further details on the origin and contribution of the α and β parameters to the overall conductance in eqn (1).

Electrolyte preparation

All electrolyte solutions, KCl and LiCl (213233, Sigma Aldrich), were prepared using ultra-pure water (ARS-105 Aries high purity water systems, resistivity of >18 MΩ cm). All LiCl electrolytes were buffered with 10 mM Tris buffer (J61036, Fisher Scientific). The pH was adjusted by adding concentrated HCl (H1758, Sigma-Aldrich) or KOH (306568, Sigma-Aldrich) dropwise and measured with an Orion Star™ pH meter.

Electrical measurements

Axopatch 200B (Molecular Devices LLC) was used for electrical measurements. A PCIe-6321 (controlled through a custom LabVIEW script (version 2016, National Instruments)) connected to a BNC 2110 (National Instruments) was used to digitize the output for *I–V* measurements. Signal digitization was carried out using a Digidata 1440A (Molecular Devices LLC) for translocation experiments. Current traces were acquired at a sampling frequency of 250 kHz and lowpass filtered at 10 kHz using the in-built Bessel filter of the Axopatch 200B.

Nanopore-based biomolecule measurements

After nanopore fabrication, baseline profiles (before the addition of hSTf to the *cis* side) were obtained for each electrolyte concentration of LiCl and KCl across all operational applied voltages (±50 mV to ±800 mV). All baseline profiles were free of any resistive pulse-like perturbations. The hSTf was purchased from Sigma Aldrich (T0665). The hSTf stock solution was stored at ~5 °C and used within 7 days from preparation. The hSTf was added to the *cis* side to a final concentration of ~100 nM. The experiments were carried out using 500 mM (~4.1 S m^{-1}), 1 M (~7.4 S m^{-1}), 1.5 M (~11.1 S m^{-1}), 2 M (~12.4 S m^{-1}), 2.5 M (~13.8 S m^{-1}), 3 M (~15.2 S m^{-1}) and 4 M (~17.6 S m^{-1}) LiCl or 500 mM (~5.9 S m^{-1}), 1 M (~11.1 S m^{-1}), 1.5 M (~15.9 S m^{-1}), 2 M (~20.9 S m^{-1}), 2.5 M (~27.9 S m^{-1}), 3 M (~32.9 S m^{-1}) and 4 M (~40.7 S m^{-1}) KCl buffered at pH 8. Single nanopores of ~14 nm diameter fabricated on ~12 nm thick silicon nitride membranes were used for translocation experiments. Events were analyzed using a custom script written in MATLAB (version 9.4). Three key parameters were extracted for a given event: baseline current (I_0), the magnitude of current perturbation (ΔI) and event duration (Δt). The Δt was calculated using the full width at the half maximum (FWHM) approach as discussed in ESI Section 1.†

Zeta potential measurements

Measurements were obtained using a Zetasizer Nano ZS (Malvern Instruments) using the procedure described in our previous work.[3] The hSTf was dissolved to a final concentration of ~25 μM in 50 mM LiCl (0.573 S m^{-1}), 50 mM KCl (0.729 S m^{-1}) and KCl at 0.573 S m^{-1} (conductivity equivalent of 50 mM LiCl). The refractive index, dielectric constant and viscosity were selected as 1.662, 80.4 and 0.87 cP for LiCl and 1.488, 80.4 and 0.89 cP for KCl, respectively. The data were treated with the Smoluchowski model in the operating software. A total of 10 cycles were performed for each electrolyte type.

Results and discussion

Solid-state nanopore experimental setup and change in conductance

The holo form of hSTf was added to the *cis* side of the nanopore and driven across the pore in response to a voltage (V_{app}) applied to the *trans* side as seen in Fig. 1a. Fig. 1b shows the directions of electrophoresis and electroosmosis originating from the interplay of the nanopore surface charge and positive V_{app}. These directions would be reversed under a negative V_{app}. For a molecule to translocate through a nanopore, it should (i) diffuse from the bulk to the capture zone of the nanopore, (ii) funnel (drift dominant) to the pore entrance, and (iii) overcome entropic (in case of long-chain polymeric molecules) and/or electrostatic barriers. If the V_{app} is not sufficient to overcome these energetic barriers, the molecule could simply collide with the pore entrance rather than translocating through it. Generally, the transport would either be diffusion-limited or barrier-limited. The diffusion-limited paradigm is typically seen with long-chain molecules under a high electric field whereas the barrier limited paradigm is typically observed with short molecules under a weak electric field. The C_R and V_{app} would be linearly correlated in the case of diffusion-limited transport (*i.e.*, Smoluchowski's rate equation) whereas the relationship is exponential in the case of barrier limited transport (*i.e.*, van't Hoff–Arrhenius formalism). The V_{app} would also dictate the translocation time (τ) and 3D structure (*e.g.*, voltage driven protein unfolding, soft particle electro-deformation) to a large extent. Using hSTf as the model molecule, we first investigated the translocation behavior across an appreciably wide V_{app} range (±50 mV to ±800 mV) using the two ubiquitous electrolytes in nanopore technology (LiCl and KCl buffered at pH ~8) as seen in Fig. 2a–f. The experiments were initially conducted with 4 M and 1 M of LiCl and 2 M of KCl. Experiments with 4 M KCl could not be conducted over the entire V_{app} range (overloads the Axopatch 200B system) while 1 M KCl yielded extremely poor C_R. At lower electrolyte concentrations, the contributions from electroosmosis and the analyte-counterions to the overall pore conductance during confinement increase. The former (*i.e.*, electroosmosis) opposes the electrophoretic motion in the case of hSTf and CT-CDB fabricated pores, and the latter increases the overall ions available for conductance. These would cause a decrease in C_R and the signal-to-noise ratio (SNR) of the resistive pulse, respectively. Lower SNR could also lead resistive pulses to be not detected by the algorithm leading to a decrease in C_R. Thus, we chose 2 M KCl, 4 M LiCl and 1 M LiCl for further investigation. A broad range of concentrations were later investigated as seen in Fig. 3 with a single V_{app} rather than a range. The initial investigation with 2 M KCl, 4 M LiCl and 1 M LiCl was to find a suitable V_{app} for the study depicted in Fig. 3.

Events were only observed for positive V_{app} for 2 M KCl, and 4 M LiCl whereas in 1 M LiCl it is the opposite polarity that

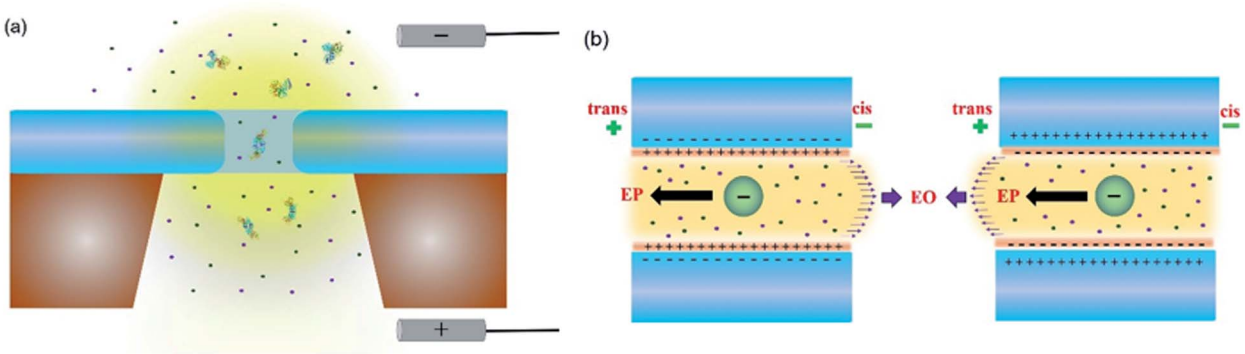

Fig. 1 (a) Schematic of a nanopore setup where the analyte is added to the *cis* side and transported across the nanopore in response to a voltage bias applied on the *trans* side. (b) The electrophoretic and electroosmotic transport mechanisms could be (left) competitive or (right) reinforcing depending on the surface charge of the nanopore and the net charge of the analyte.

generated events (Fig. S2†). The change in response to the V_{app} polarity is attributed to the change in the transport mechanism (*i.e.*, from electrophoresis at high LiCl concentrations to electroosmosis at low LiCl concentrations). In all three electrolyte conditions, the C_R with V_{app} exhibited two distinct linear regimes (*i.e.*, a breakpoint at ~400 mV). While 2 M KCl (Fig. 2a) demonstrated a higher sensitivity (*i.e.*, higher slope) after the breakpoint (~2.5× compared to pre-breakpoint slope), in 4 M LiCl (Fig. 2b), the sensitivity dropped by ~1.8× after the breakpoint. Interestingly, with 1 M LiCl (Fig. 2c) an inverse relationship between C_R and V_{app} was observed after the breakpoint. The change in conductance due to hSTf translocation ($\Delta G_{p,f}$) decreased with increasing V_{app} and plateaued at ~400 mV in 2 M KCl while it continued to drop in the other two cases (Fig. 2d). The ΔG_p was calculated by fitting a Gaussian mixture model to the histogram distribution of change in open pore current (ΔI) as outlined in ESI Section 3.† The nonlinear behavior of $\Delta G_{p,f}$ with V_{app} is indicative of voltage-driven unfolding and the plateauing is indicative of maximum possible unfolding under the experimental conditions.[3,41] An unfolded protein is typically more surface charged than its folded counterpart due to the exposure of charged moieties that are otherwise hidden due to folding.[42] According to the Hofmeister series, Li^+ is a chaotropic cation while K^+ is a kosmotropic cation.[43] It is possible that with voltage-driven unfolding, the ions of the electrolyte would have more access to the otherwise shielded moieties due to the folded structure with chaotropic cations denaturing and destabilizing the protein structure compared to kosmotropic cations. Although, the unfolding plateaus in 2 M KCl (V_{app} > 400 mV), the continued unfolding in both 4 M and 1 M LiCl could be due to these chaotropic effects of Li^+. Taken together, these could provide explanations to the change in slope after the breakpoint in Fig. 2a–c: (i) exposure of charged moieties through protein unfolding would increase the contribution to electrophoretic movement and thereby increasing the capture probability, (ii) chaotropic destabilization would reduce the number of detectable molecules which would increase with additional unfolding contributions. For example, an extra degree of unfolding component could be introduced due to the opposing electroosmosis (dominant transport mechanism) and electrophoresis mechanisms in the case of 1 M LiCl (Fig. 2c) which would further destabilize the protein structure and by extension the detectable molecules. The increase in the molecular length of hSTf caused by voltage-driven unfolding would also minimize fast translocations that defy the electronic limitations of the Axopatch system (*i.e.*, more molecules are detected) and would also lead to an increase in τ with V_{app} as seen in Fig. 2f and has been observed previously as well.[3] As expected, the opposing electroosmotic and electrophoretic forces lead to a higher τ in 1 M LiCl as evident by Fig. 2f (blue trace). However, we note that the bandwidth limitations of the Axopatch 200B amplifier may cause ballistic events to be not detected and only those that are delayed through interactions with the pore to be detected as noted by previous work in the literature.[44] To affirm the missed events, we first calculated the effective capture radius (r_{eff}) using $r_{eff} = C_R/2\pi DC$ where D and C are bulk diffusion coefficient (estimated using the Stokes–Einstein equation and was found to be $\sim 7.6 \times 10^{-7}$ cm^2 s^{-1} for hSTf) and hSTf concentration (~100 nM) respectively. The r_{eff} at ±400 mV was found to be ~1 nm, ~0.6 nm and ~0.9 nm in 2 M KCl, 4 M LiCl and 1 M LiCl respectively which is at least 14× smaller than the pore radius. While high bandwidth equipment would permit to detect fast moving protein events, as noted by Tabard Cossa *et al.*, we obtained statistically significant data (>1000 events) across all events to draw conclusions based on events slowed down through interactions with the pore.[44]

At higher electric fields, experiments with 0.5 M LiCl were not possible for two reasons: persistent clogging and poor C_R at high electric fields. Moreover, as mentioned, hSTf continues to unfold beyond 400 mV in 4 M LiCl and 1 M LiCl while $\Delta G_{p,f}$ plateaus at ~400 mV in 2 M KCl. Furthermore, the capture rate in 1 M LiCl drops at voltages higher than 400 mV. Taking the above observations of the voltage-dependent study into account, we decided to conduct further studies at ±400 mV for the electrolyte concentration range from 1–4 M. The resistive pulses (also called events) in response to ±400 mV applied voltages are shown in Fig. 3a and b for 1–4 M LiCl and KCl (buffered at pH ~8), respectively. The corresponding scatter plots are shown in Fig. 3c (LiCl) and Fig. 3d (KCl). Selected

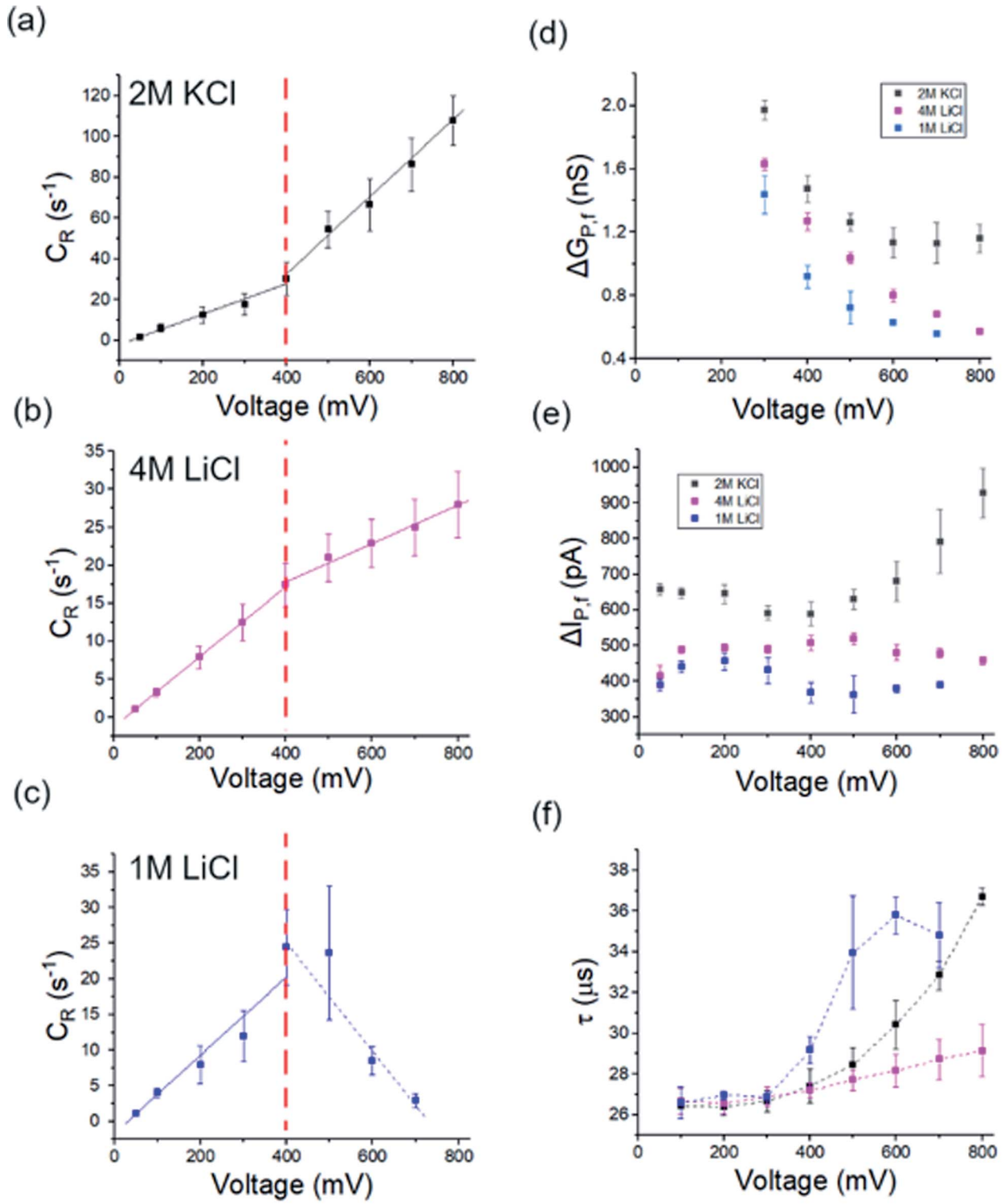

Fig. 2 (a–c) capture rate (C_R), (d) conductance change ($\Delta G_{p,f}$), (e) open-pore current change ($\Delta I_{p,f}$), and (f) translocation time (τ) originating from hSTf translocation as a function of applied voltage in 2 M KCl (black), 4 M LiCl (magenta) and 1 M KCl (blue) respectively. All experiments were conducted at pH ~8 using ~14 nm diameter pores. Note that all voltages corresponding to 1 M LiCl are in negative polarity whereas the rest (*i.e.*, 2 M KCl and 4 M LiCl) are in positive polarity. Solid lines in (a–c) are linear fits to raw data points (on either side of the red vertical line). Three independent runs to replicate experiments were performed with new samples across two unique nanopores of similar size. Full length of each error bar corresponds to the standard deviation of the replicated measurements.

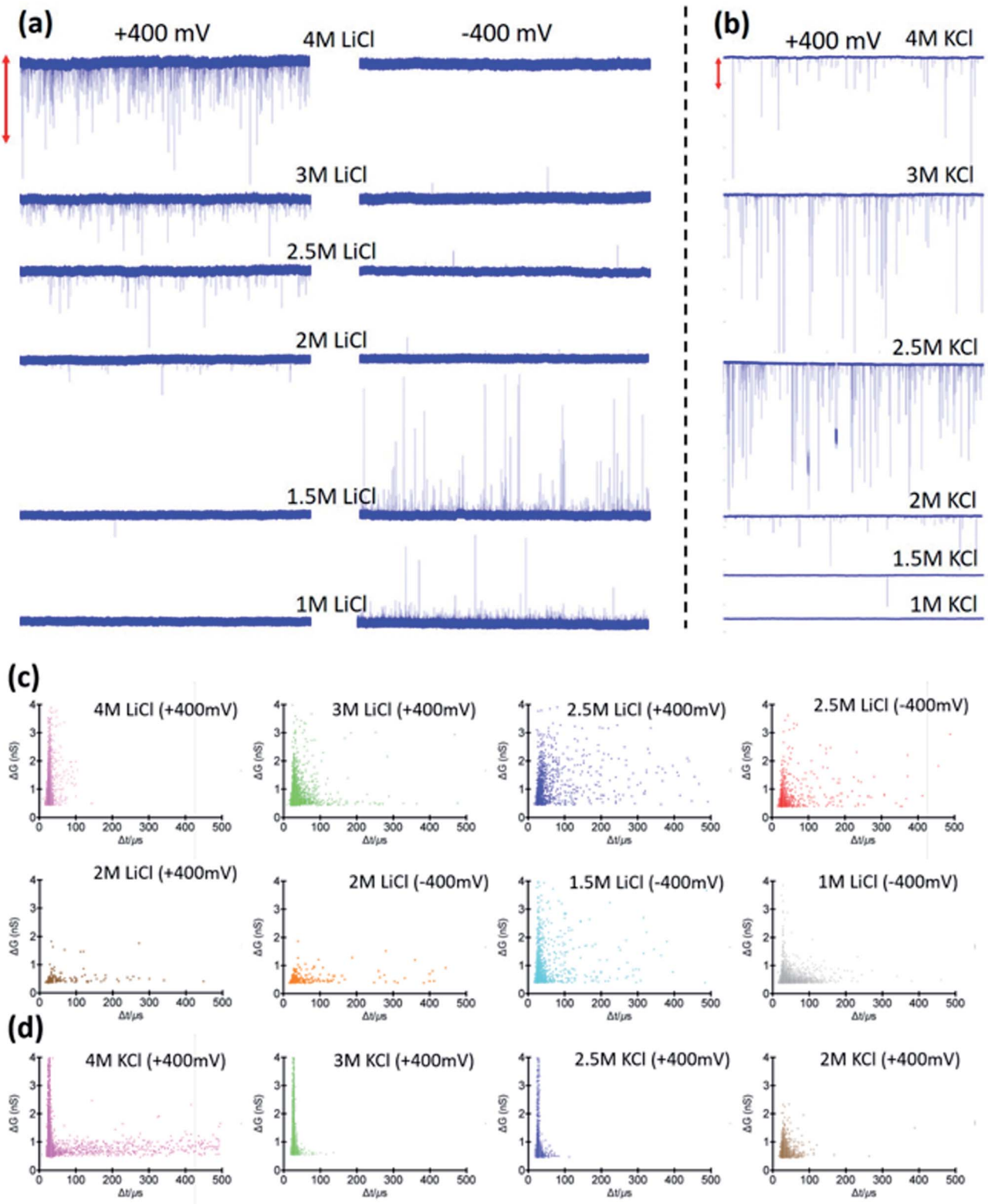

Fig. 3 25 second current traces corresponding to hSTf translocations in (a) LiCl under applied voltages of (left column) +400 mV and, (right column) −400 mV and (b) KCl under applied voltage of +400 mV at pH ~8. Traces corresponding to −400 mV for KCl are not shown as there were no events in negative polarity. The vertical bar at the top corresponds to 2000 pA (LiCl) and 5000 pA (KCl). Scatter plots corresponding to change in conductance because of analyte transit with the corresponding translocation time for 4 M, 3 M, 2.5 M, 2 M, 1.5 M, and 1 M of (c) LiCl and (d) 4 M, 3 M, 2.5 M and, 2 M of KCl buffered at pH ~8. All experiments were conducted using ~14 nm diameter pores.

extended current traces are shown in Fig. S3 and S4,† which showcase the stability of CT-CDB nanopores and their resilience to lengthy experiments spanning a considerable number of sensing conditions (Fig. S5† shows the response at ±50 mV for 0.5–4 M LiCl and KCl with selected extended current traces shown in Fig. S6 and S7†). Thus, the concentration analysis was limited to 1–4 M at ±400 mV. Interestingly, as seen in Fig. 3b, KCl showed events only for +400 mV across all concentrations whereas LiCl (Fig. 3a) showed a transition from being solely responsive to +400 mV at higher concentrations (electrophoresis-dominant transport mechanism), to both polarities at intermediate concentrations and solely responsive to −400 mV at lower concentrations (electroosmosis-dominant transport mechanism). The zeta potential of the protein (hSTf in this case) and the nanopore for each electrolyte type and concentration is believed to play a vital role in the transport direction. Considering the zeta potential of hSTf (ζ_{hSTf}) and that of the nanopore wall (ζ_{pore}), the resultant drift velocity of hSTf can be expressed as $\upsilon_{hSTf} = \frac{\varepsilon(\zeta_{hSTf} - \zeta_{pore})}{\eta}E$ where E, ε and η are average electric field strength, solution permittivity and viscosity of the medium, respectively.[45] The quantity $\zeta_{hSTf} - \zeta_{pore}$ would to a large extent determine whether the mechanism is electroosmotic ($\zeta_{hSTf} < \zeta_{pore}$) or electrophoretic ($\zeta_{hSTf} > \zeta_{pore}$) dominated and is more broadly discussed below.

Transport mechanism and capture based zeta potential measurement

To quantitatively assess the transport mechanism, ζ_{hSTf} must be compared against ζ_{pore}. At high salt concentrations (smaller Debye length compared to pore radius), ζ_{pore} could be calculated using an approximate extension of Grahame equation (see ESI Section 4† for further information),

$$\zeta_{pore} = \frac{\sigma_p}{\varepsilon_r \varepsilon_0}\kappa^{-1} \quad (2)$$

where κ^{-1}, ε_r and ε_0 are Debye screening length, relative permittivity, and vacuum permittivity, respectively. To deduce σ_p, the open-pore conductance (G) of ~13.5 ± 0.5 nm diameter pores were measured as a function of the electrolyte concentration and fitted with eqn (1) as shown in Fig. 4a (in LiCl) and 4b (in KCl). The σ_p in LiCl ($\sigma_{p,LiCl}$) and KCl ($\sigma_{p,KCl}$) were found to be $\sim -84.1 \pm 6.1$ mC m^{-2} and $\sim -78.9 \pm 9.9$ mC m^{-2} respectively. This indicates that σ_p does not change appreciably with the electrolyte type and the observed differences between hSTf transport in LiCl and KCl electrolyte could be mainly due to hSTf–electrolyte interactions. One must also be attentive to the fact that ζ_{pore} depends on the process chemistry by which the membranes are fabricated and by extension the host of physiochemical factors that underscore the origin of ζ_{pore}. Thus, it is prudent to construct figures resembling 4a and b even for pores that are fabricated through the same membrane-type using different methods since the fabrication method has been shown to affect the final pore chemistry.[27] These σ_p values were then used to calculate ζ_{pore}using eqn (2) for each of electrolyte concentrations of KCl and LiCl (see Table S1† for the calculated values).

ζ_{hSTf} was also estimated using a Zetasizer (see Methods section for more details).[46–48] The measured values are shown in Table S2† and support the notion of LiCl shielding the charge of the charged biomolecules compared to KCl.[49] Although these values are in agreement with what we have obtained previously,[3] it only satisfy the $\zeta_{hSTf} < \zeta_{pore}$ condition which suggests that the transport mechanism should be electroosmosis-dominant across all electrolyte concentrations (see Table S1† for tabulated ζ_{pore} values). However, as seen in Fig. 3a, this is not the case where a clear shift in the mechanism from electrophoresis to electroosmosis was observed with decreasing LiCl concertation (with KCl been purely electrophoretic). Thus, even when providing the correct sign, the magnitude of zeta-potential measurements may not be accurate to describe the observed results. Although nanopore-based zeta potential calculation is possible,[46–48] missed events arising from the bandwidth limitation of the Axopatch 200B impede the proper estimation of electrophoretic mobility essential for such calculations. Our efforts to calculate ζ_{hSTf} through the translocation time based nanopore methods outlined in literature corroborated this notion where the calculated values in 2 M KCl and 4 M LiCl were in unrealistic sub-μV regime (calculations not shown). Due to the shortcomings of the ζ_{hSTf} estimation through above methods, we present a C_R *vs.* ζ_{pore} method to calculate ζ_{hSTf}. Interestingly, the C_R of hSTf in KCl (unlike LiCl) drops at higher concentrations as seen in Fig. 4c while C_R in LiCl showed a linear dependence. This result also supports the notion that electrolyte chemistry and V_{app} should be chosen with utmost care since proteins, unlike rigid particles and DNA undergo significant molecular level changes especially with V_{app}. Hereafter, we limit the discussion to LiCl. To quantify the observed capture rates, we resorted to the diffusion-limited capture rate (R_{diff}) which is given by $\frac{\pi {r_0}^2 \mu}{L}\Delta V$.[50] The electrophoretic mobility (μ) can be expressed using apparent zeta potential and the dielectric constant of the medium (ε_d) as $\frac{\varepsilon_d(\zeta_{hSTf} - \zeta_{pore})}{\eta}$.[45] Thus, R_{diff}can now be expressed as,

$$R_{diff} = \frac{\pi {r_0}^2}{L}\frac{\varepsilon_d(\zeta_{hSTf} - \zeta_{pore})}{\eta}\Delta V \quad (3)$$

Using each of the linear fit lines shown in Fig. 4d, one can calculate the ζ_{hSTf} when R_{diff} approaches zero ($R_{diff} \rightarrow 0$). The zeta potential of hSTf at $R_{diff} \rightarrow 0$ point ($\zeta_{hSTf}^{r_{events} \rightarrow 0}$) was found to be −26.2 mV (black trace, electrophoresis dominant fit) and −25.2 mV (magenta trace, electroosmosis dominant fit): both yielded appreciably close zeta potential values that are much greater than those obtained from the Zetasizer. A zeta potential <−30 mV generally indicates an unstable solution where analytes tend to aggregate irreversibly[51] and given the fact $\zeta_{hSTf}^{r_{events} \rightarrow 0} \sim -30$ mV, hSTf may be stable under the experimental conditions of Fig. 4d. Since LiCl produced statistically significant event counts across all electrolyte concentrations, $R_{diff} \rightarrow 0$ may not be the best way to determine ζ_{hSTf}. Eqn (3) can be separated into electrophoretic and electroosmotic components

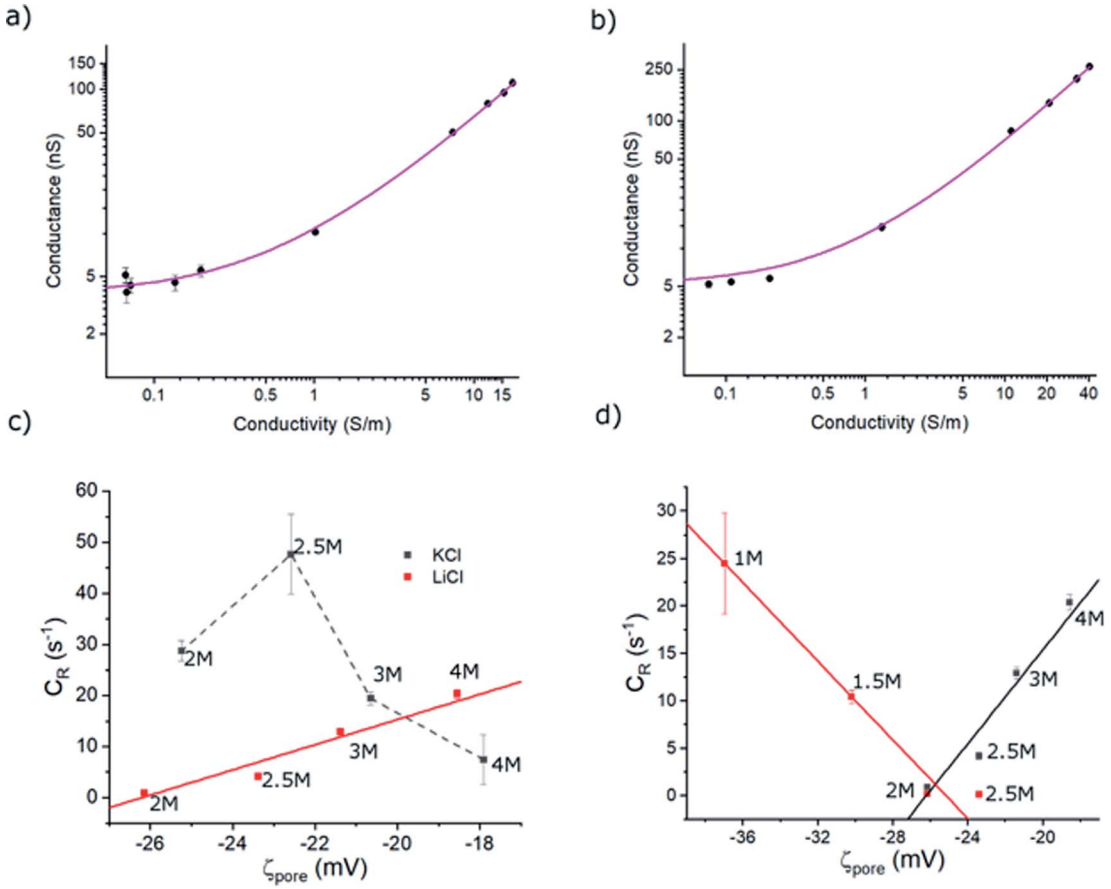

Fig. 4 Open-pore conductance (G) as a function of (a) LiCl conductivity and (b) KCl conductivity. The solid line in each is the best fit to the data made using eqn (1) with σ_p as the sole free parameter. Full length of each error bar corresponds to the standard deviation of the replicated measurements. (c) Event rate of hSTf in KCl (black) and LiCl (red) with the zeta potential of the nanopore surface (ζ_{pore}) from 4 M to 2 M electrolyte concentrations at +400 mV applied voltage. (d) Event rate of hSTf in 1 M to 4 M LiCl in response to +400 mV (black) and −400 mV (red). The electrolyte concentrations of (c) and (d) are indicated adjacent to the corresponding data point.

as $\frac{\pi {r_0}^2 \varepsilon_d \Delta V}{L\eta}\zeta_{hSTf}$ ($R_{diff,EP}$) and $\frac{\pi {r_0}^2 \varepsilon_d \Delta V}{L\eta}\zeta_{pore}$ ($R_{diff,EO}$) respectively. Since the transport direction depends on the difference in the zeta potential of the nanopore surface and the analyte (*i.e.*, $\zeta_{hSTf} - \zeta_{pore}$), when the condition $\zeta_{pore} \approx \zeta_{hSTf}$ is satisfied, the event rate is expected to approach zero provided diffusion alone does not lead to an appreciable event rate. To check the validity of this claim, we first calculated the frequency factor (R_{f0}) from the barrier penetration using, $R_{f0} = CDA/l$ where C, D and A are bulk concentration of hSTf, diffusion coefficient of hSTf and the cross-sectional area of the channel.[52] For a ~14 nm diameter pore through a 12 nm thick membrane with 100 nM hSTf, R_{f0} was found to be ~12.4 s^{-1} (D was estimated using the Stokes–Einstein equation and was found to be ~7.6 × 10^{-7} cm^2 s^{-1} for hSTf). Using event rate at the intersection point (~1.2 s^{-1}) the activation energy (U) was found to be ~2.4k_BT using $R_0 = k \times R_{f0} \exp(-U/k_BT)$ with R_0, k and k_B the activation energy (U) governed zero voltage capture rate, probability factor (assumed to be 1) and Boltzmann constant.[52–54] Since $U > k_BT$ we wouldn't expect diffusion alone to produce an appreciable C_R. The intersection point in Fig. 4d ($R_{diff,EP} = R_{diff,EO}$) may in fact be a better representation of ζ_{hSTf}. The ζ_{pore} at this intersection point was found to be ~ −25.7 mV ($\zeta_{hSTf}^{EP=EO}$). The ζ_{hSTf} can also be used to estimate the net charge of the protein assuming spherical shape of the protein and uniformly distributed surface charge.[55] We used a similar framework at a weaker electric field ($V_{app} = \pm 50$ mV) from which $\zeta_{hSTf}^{EP=EO}$ was found to be ~ −25.9 mV (Fig. S11†). However, one must understand that eqn (3) is not properly applicable to weak electric fields. At lower voltages (*i.e.*, voltage approaching 0 mV), the transport mechanism become barrier limited. In such cases, the Van't Hoff–Arrhenius formalism is more applicable which is given by $R_{bar} = k \times R_{f0} \exp(-(U - \Delta U)/k_BT)$, where R_{bar} and ΔU, are the barrier-limited capture rate and, activation energy, respectively. The ΔU is typically given by $q\Delta V$ where q and ΔV are the effective charge of the molecule and applied voltage to the electrodes. Thus, with increasing applied voltage, the capture rate would expect to increase exponentially. However, if the limiting case of translocation is diffusion, the eqn (3) is applicable and a linear increase of capture rate with applied voltage is observed.

Modeling of change in conductance

As our previous study with hSTf showed voltage-driven unfolding of protein with increasing applied voltage,[3] to minimize

such, we now operated at a low V_{app} (±50 mV) using 0.5–4 M LiCl.[3] The change in conductance because of hSTf translocations exhibited a bimodal distribution (see Fig. S12 and ESI Section 3† for fit details). The lower ΔG ($\Delta G_{p,c}$) did not show a significant dependence on the electrolyte conductivity whereas the higher ΔG ($\Delta G_{p,f}$) showed a proportional relationship with electrolyte conductivity (Fig. S13†). The $\Delta G_{p,f}$, given the low applied voltage, could correlate to globular-like translocations since voltage-driven unfolding would be negligible at weak electric fields (*i.e.*, the protein is closer to its native state). If we disregard surface contributions – both from pore wall and particle – the conductance change of the second population ($\Delta G_{p,f}$) can be expressed as;

$$\Delta G_{p,f} = K\frac{\gamma \cdot \Lambda}{(L+1.6r_0)^2}S_{r,d} \quad (4)$$

where Λ, γ, and $S_{r,d}$ are the excluded volume, shape factor (assumed to be 1.5 for spheres),[56] and the correction factor (dependent on the relative values of the nanopore and molecular radii and assumed to be 1). As seen through the derivation shown in ESI Section 6,† it is evident, eqn (4) holds only for spherical particles. However, caution should be exercised when analyte and pore radii become comparable as eqn (S5) (and by extension eqn (S6)†) may not hold true. Although it is a common practice to use eqn (4) to model $\Delta G_{p,f}$, at low salt concentrations, the surface charge effects must be considered to better estimate $\Delta G_{p,f}$.[48] Furthermore, eqn (4) was initially derived about five decades ago for micron-scale tubes (eqn (S10)†) but not for nanopores.[57] The numerical assignment for γ (1.5) is purely based on mathematical manipulation (eqn (S11)†) arising by considering the transiting molecule as a sphere and therefore assigning a value other than 1.5 needs substantial shape-dependent refinement for the derivation that leads to eqn (4) (see ESI Section 6† for a detailed discussion). Therefore, considering γ as a variable in the current form of eqn (4) – a common practice in literature – is questionable as well. Detailed information regarding the assumptions related to eqn (4) and various models used to estimate conductance change can be found elsewhere.[58,59] Circumventing the limitations of eqn (4), $\Delta G_{p,f}$ for a protein with a radius r_p translocating through a pore with radius r_0 and length L submerged in an electrolyte of conductivity K was derived to be (see ESI Section 6† for the detailed derivation),

$$\Delta G_{p,f} = G - K_{eff}\left(\frac{1}{\frac{\pi {r_0}^2}{L}+\frac{\mu|\sigma|}{K_{eff}}\times\frac{2\pi r_0}{L}}+\frac{2}{\alpha\times 2r_0+\beta\times\frac{\mu|\sigma|}{K_{eff}}}\right)^{-1} \quad (5)$$

where K_{eff} is the effective conductivity for a pore with an insulating sphere in a solution with conductivity K. As shown in eqn (S15) in ESI Section 6,† Using Maxwell's approximation, K_{eff} can be written in terms of volume fraction (f) of an insulating sphere $\left(\frac{4{r_p}^3}{3{r_0}^2L}\right)$ in a solution with conductivity, K can be expressed as $K_{eff} = \frac{K}{\left(1+\frac{3}{2}f+\ldots\right)}$. The raw data ($\Delta G_{p,f}$) was fitted with both eqn (4) ($S_{r,d}$ set to 1, Fig. 5a) and eqn (5) (Fig. 5b). The resulting r_p values were ~3.84 (eqn (4)) and ~3.14 (eqn (5)). While both models yielded similar R^2 values (~0.987), the r_p value produced by our model (eqn (5)) is in close agreement with the reported value for hSTf based on its molecular volume (~3.2 nm).[3,38] For simplicity, in eqn (5), we have neglected contributions from the protein charge as proteins do not have a uniform charge or shape. Further refinement of eqn (5), we believe, is beyond the scope of this paper, as it would require substantial analytical modelling.

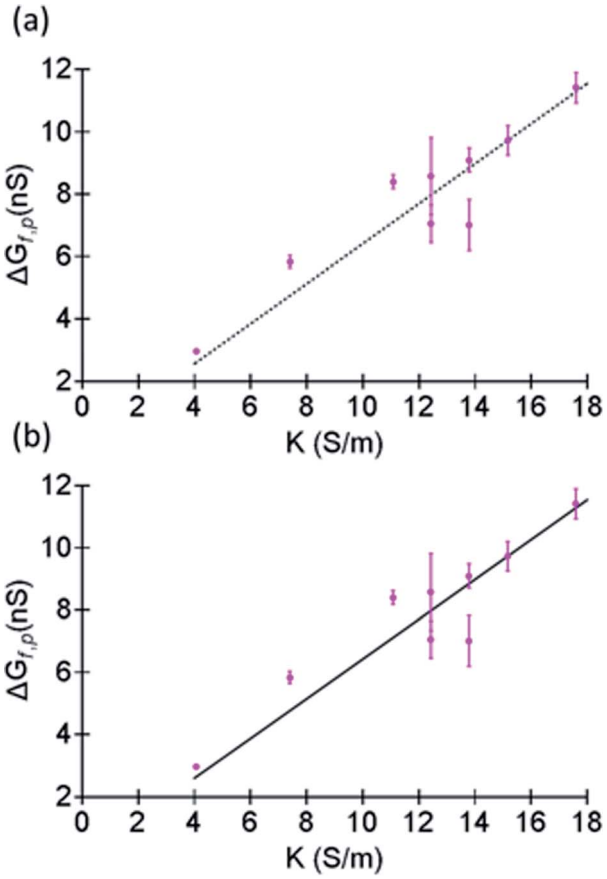

Fig. 5 Fits made to $\Delta G_{p,f}$ (corresponding to the histograms shown in Fig. S12†) as a function of the conductivity of LiCl at pH ~8 using (a) eqn (4) and (b) eqn (5) with r_p as the free parameter. The fit was done by having r_p as the sole free parameter. In the case of eqn (4), $S_{r,d}$ and γ were set to 1 and 1.5 respectively and Λ was substituted by the volume of a sphere. Full length of each error bar corresponds to the standard deviation of the replicated measurements.

Conclusions

In this study, we have demonstrated the responsiveness of the holo form of hSTf in LiCl and KCl concentrations ranging from 4 M to 0.5 M at pH ~8, using silicon nitride nanopores fabricated through the CT-CDB process. While the responsiveness was found to be purely electrophoretic for KCl, in LiCl, a transition from electrophoretic to electroosmotic was observed at low electrolyte concentrations (typically <2 M) while at

intermediate concentrations (*e.g.*, 2 M and 2.5 M) events were observed for both voltage polarities suggesting diffusion plays a vital role in the translocation mechanism at such concentrations. To further understand this reversal of translocation mechanism with decreasing electrolyte concentration, the zeta potential of both the nanopore surface (ζ_{pore}) and holo-hSTf (ζ_{hSTf}) were calculated. The ζ_{pore} was calculated by surveying the open pore nanopore conductance (G) with electrolyte concentration and by fitting the raw data with eqn (1) to obtain the surface charge density (σ_p). Then ζ_{pore} was calculated for the range of LiCl and KCl concentrations used herein. The ζ_{hSTf} was measured (Zetasizer) and subsequently calculated using the correlation between ζ_{pore} and the diffusion-limited capture rate (R_{diff}). We used the relationship between R_{diff} and ζ_{pore} as an alternative way to estimate ζ_{hSTf}. By extrapolating the R_{diff} to zero (point where $\zeta_{pore} \approx \zeta_{hSTf}$), the ζ_{hSTf} found ($\zeta_{hSTf}^{r_{events} \to 0}$). Although mathematically R_{diff} can be extrapolated to zero, for electrolytes such as LiCl, it is not a pragmatic approximation as events are produced for either voltage polarity under the concentration range considered in this study. Therefore, we looked at the event rate components corresponding to electrophoresis ($R_{diff,EP}$) and electroosmosis ($R_{diff,EO}$) and determined the ζ_{pore} at which the two contributions become equal (the intersection point of the rate profiles). The ζ_{hSTf} at the intersection point ($\zeta_{hSTf}^{EP=EO}$) was found to be ~25.7 mV. We then ventured into modelling the conductance change (ΔG) because of hSTf translocations. The conventionally used eqn (4) was found to have shortcomings for its adaptation to nanopore-based profiling and a new equation was proposed to quantify the conductance change due to protein translocation process (eqn (5)).

Conflicts of interest

The authors have declared no conflict of interest.

Acknowledgements

This work was supported by the National Science Foundation (CBET #2022398 and #2022374) and National Institutes of Health (R21CA240220).

References

1 K. J. Freedman, C. W. Ahn and M. J. Kim, Detection of long and short DNA using nanopores with graphitic polyhedral edges, *ACS Nano*, 2013, **7**, 5008–5016.
2 J. Feng, K. Liu, R. D. Bulushev, S. Khlybov, D. Dumcenco, A. Kis and A. Radenovic, Identification of single nucleotides in MoS_2 nanopores, *Nat. Nanotechnol.*, 2015, **10**, 1070.
3 J. Saharia, Y. N. D. Bandara, G. Goyal, J. S. Lee, B. I. Karawdeniya and M. J. Kim, Molecular-Level Profiling of Human Serum Transferrin Protein through Assessment of Nanopore-Based Electrical and Chemical Responsiveness, *ACS Nano*, 2019, **13**, 4246–4254.
4 J. Saharia, Y. N. D. Bandara, J. S. Lee, Q. Wang, M. J. Kim and M. J. Kim, Fabrication of hexagonal boron nitride based 2D nanopore sensor for the assessment of electro-chemical responsiveness of human serum transferrin protein, *Electrophoresis*, 2020, **41**, 630–637.
5 K. J. Freedman, M. Jürgens, A. Prabhu, C. W. Ahn, P. Jemth, J. B. Edel and M. J. Kim, Chemical, thermal, and electric field induced unfolding of single protein molecules studied using nanopores, *Anal. Chem.*, 2011, **83**, 5137–5144.
6 Y. M. N. D. Y. Bandara, J. Tang, J. Saharia, L. W. Rogowski, C. W. Ahn and M. J. Kim, Characterization of Flagellar Filaments and Flagellin through Optical Microscopy and Label-Free Nanopore Responsiveness, *Anal. Chem.*, 2019, **91**, 13665–13674.
7 B. I. Karawdeniya, Y. N. D. Bandara, J. W. Nichols, R. B. Chevalier, J. T. Hagan and J. R. Dwyer, Testing, Challenging Nanopores with Analyte Scope and Environment, *J. Anal. Test.*, 2019, **3**, 61–79.
8 B. I. Karawdeniya, Y. N. D. Bandara, J. W. Nichols, R. B. Chevalier and J. R. Dwyer, Surveying silicon nitride nanopores for glycomics and heparin quality assurance, *Nat. Commun.*, 2018, **9**, 3278.
9 H. Wu, Y. Chen, Q. Zhou, R. Wang, B. Xia, D. Ma, K. Luo and Q. Liu, Translocation of rigid rod-shaped virus through various solid-state nanopores, *Anal. Chem.*, 2016, **88**, 2502–2510.
10 L. Liu, H. Wu, J. Kong and Q. Liu, Solid-state nanopore for rod-like virus detection, *Sci. Adv. Mater.*, 2013, **5**, 2039–2047.
11 B. I. Karawdeniya, Y. M. N. D. Y. Bandara, A. I. Khan, W. T. Chen, H.-A. Vu, A. Morshed, J. Suh, P. Dutta and M. J. Kim, Adeno-associated virus characterization for cargo discrimination through nanopore responsiveness, *Nanoscale*, 2020, **12**, 23721–23731.
12 A. Darvish, G. Goyal, R. Aneja, R. V. Sundaram, K. Lee, C. W. Ahn, K.-B. Kim, P. M. Vlahovska and M. J. Kim, Nanoparticle mechanics: deformation detection *via* nanopore resistive pulse sensing, *Nanoscale*, 2016, **8**, 14420–14431.
13 J. S. Lee, J. Saharia, Y. N. D. Bandara, B. I. Karawdeniya, G. Goyal, A. Darvish, Q. Wang, M. J. Kim and M. J. Kim, Stiffness measurement of nanosized liposomes using solid-state nanopore sensor with automated recapturing platform, *Electrophoresis*, 2019, **40**, 1337–1344.
14 G. Goyal, A. Darvish and M. J. Kim, Use of solid-state nanopores for sensing co-translocational deformation of nano-liposomes, *Analyst*, 2015, **140**, 4865–4873.
15 M. Chinappi, M. Yamaji, R. Kawano and F. Cecconi, Analytical model for particle capture in nanopores elucidates competition among electrophoresis, electroosmosis, and dielectrophoresis, *ACS Nano*, 2020, **14**, 15816–15828.
16 A. Asandei, I. Schiopu, M. Chinappi, C. H. Seo, Y. Park and T. Luchian, Electroosmotic trap against the electrophoretic force near a protein nanopore reveals peptide dynamics during capture and translocation, *ACS Appl. Mater. Interfaces*, 2016, **8**, 13166–13179.

17 K. Tian, K. Decker, A. Aksimentiev and L.-Q. Gu, Interference-free detection of genetic biomarkers using synthetic dipole-facilitated nanopore dielectrophoresis, *ACS Nano*, 2017, **11**, 1204–1213.

18 G. Huang, K. Willems, M. Soskine, C. Wloka and G. Maglia, Electro-osmotic capture and ionic discrimination of peptide and protein biomarkers with FraC nanopores, *Nat. Commun.*, 2017, **8**, 1–11.

19 M. Firnkes, D. Pedone, J. Knezevic, M. Doblinger and U. Rant, Electrically facilitated translocations of proteins through silicon nitride nanopores: conjoint and competitive action of diffusion, electrophoresis, and electroosmosis, *Nano Lett.*, 2010, **10**, 2162–2167.

20 A. Squires and A. Meller, DNA Capture and Translocation through Nanoscale Pores—a Fine Balance of Electrophoresis and Electroosmosis, *Biophys. J.*, 2013, **105**, 543–544.

21 R. Gasparac, D. T. Mitchell and C. R. Martin, Electrokinetic DNA transport in a nanopore membrane, *Electrochim. Acta*, 2004, **49**, 847–850.

22 A. Y. Grosberg and Y. Rabin, DNA capture into a nanopore: interplay of diffusion and electrohydrodynamics, *J. Chem. Phys.*, 2010, **133**, 165102.

23 D. P. Hoogerheide, S. Garaj and J. A. Golovchenko, Probing surface charge fluctuations with solid-state nanopores, *Phys. Rev. Lett.*, 2009, **102**, 256804.

24 Y. N. D. Bandara, B. I. Karawdeniya, J. T. Hagan, R. B. Chevalier and J. R. Dwyer, Chemically Functionalizing Controlled Dielectric Breakdown Silicon Nitride Nanopores by Direct Photohydrosilylation, *ACS Appl. Mater. Interfaces*, 2019, **11**, 30411–30420.

25 B. N. Anderson, M. Muthukumar and A. Meller, pH tuning of DNA translocation time through organically functionalized nanopores, *ACS Nano*, 2012, **7**, 1408–1414.

26 Y. N. D. Bandara, B. I. Karawdeniya and J. R. Dwyer, Push-Button Method To Create Nanopores Using a Tesla-Coil Lighter, *ACS Omega*, 2019, **4**, 226–230.

27 Y. M. N. D. Y. Bandara, J. Saharia, B. I. Karawdeniya, J. T. Hagan, J. R. Dwyer and M. J. Kim, Beyond nanopore sizing: improving solid-state single-molecule sensing performance, lifetime, and analyte scope for omics by targeting surface chemistry during fabrication, *Nanotechnology*, 2020, **31**, 335707.

28 J. W. Robertson, C. G. Rodrigues, V. M. Stanford, K. A. Rubinson, O. V. Krasilnikov and J. J. Kasianowicz, Single-molecule mass spectrometry in solution using a solitary nanopore, *Proc. Natl. Acad. Sci. U. S. A.*, 2007, **104**, 8207–8211.

29 R. M. Smeets, U. F. Keyser, D. Krapf, M.-Y. Wu, N. H. Dekker and C. Dekker, Salt dependence of ion transport and DNA translocation through solid-state nanopores, *Nano Lett.*, 2006, **6**, 89–95.

30 H. Bruus, *Theoretical Microfluidics*, Oxford University Press, Oxford, 2008; vol. 18.

31 C. M. Frament, N. Bandara and J. R. Dwyer, Nanopore surface coating delivers nanopore size and shape through conductance-based sizing, *ACS Appl. Mater. Interfaces*, 2013, **5**, 9330–9337.

32 J. Dwyer, Y. Bandara, J. Whelan, B. Karawdeniya and J. Nichols, Silicon Nitride Thin Films for Nanofluidic Device Fabrication, *Nanofluidics*, 2016, **41**, 190.

33 E. Y. Chi, S. Krishnan, T. W. Randolph and J. F. Carpenter, Physical stability of proteins in aqueous solution: mechanism and driving forces in nonnative protein aggregation, *Pharm. Res.*, 2003, **20**, 1325–1336.

34 D. S. Maclean, Q. Qian and C. R. Middaugh, Stabilization of proteins by low molecular weight multi-ions, *J. Pharm. Sci.*, 2002, **91**, 2220–2229.

35 J. M. Broering and A. S. Bommarius, Evaluation of Hofmeister effects on the kinetic stability of proteins, *J. Phys. Chem. B*, 2005, **109**, 20612–20619.

36 A. A. Green, Studies in the physical chemistry of the proteins X. The solubility of hemoglobin in solutions of chlorides and sulfates of varying concentration, *J. Biol. Chem.*, 1932, **95**, 47–66.

37 L. Medda, C. Carucci, D. F. Parsons, B. W. Ninham, M. Monduzzi and A. Salis, Specific cation effects on hemoglobin aggregation below and at physiological salt concentration, *Langmuir*, 2013, **29**, 15350–15358.

38 S. Welch, *Transferrin: The Iron Carrier*, CRC Press, Boca Raton, 1992, pp. 60–90.

39 I. Nir, D. Huttner and A. Meller, Direct sensing and discrimination among ubiquitin and ubiquitin chains using solid-state nanopores, *Biophys. J.*, 2015, **108**, 2340–2349.

40 C. Lee, L. Joly, A. Siria, A.-L. Biance, R. m. Fulcrand and L. r. Bocquet, Large apparent electric size of solid-state nanopores due to spatially extended surface conduction, *Nano Lett.*, 2012, **12**, 4037–4044.

41 K. J. Freedman, S. R. Haq, J. B. Edel, P. Jemth and M. J. Kim, Single molecule unfolding and stretching of protein domains inside a solid-state nanopore by electric field, *Sci. Rep.*, 2013, **3**, 1638.

42 X. Wang, M. D. Wilkinson, X. Lin, R. Ren, K. R. Willison, A. P. Ivanov, J. Baum and J. B. Edel, Single-molecule nanopore sensing of actin dynamics and drug binding, *Chem. Sci.*, 2020, **11**, 970–979.

43 B. Kang, H. Tang, Z. Zhao and S. Song, Hofmeister series: Insights of ion specificity from amphiphilic assembly and interface property, *ACS Omega*, 2020, **5**, 6229–6239.

44 A. T. Carlsen and V. Tabard-Cossa, Mapping shifts in nanopore signal to changes in protein and protein-DNA conformation, *bioRxiv*, 2020, DOI: 10.1101/2020.04.01.020420.

45 D. Y. Ling and X. S. Ling, On the distribution of DNA translocation times in solid-state nanopores: an analysis using Schrödinger's first-passage-time theory, *J. Phys.: Condens. Matter*, 2013, **25**, 375102.

46 N. Arjmandi, W. Van Roy, L. Lagae and G. Borghs, Measuring the electric charge and zeta potential of nanometer-sized objects using pyramidal-shaped nanopores, *Anal. Chem.*, 2012, **84**, 8490–8496.

47 P. Waduge, R. Hu, P. Bandarkar, H. Yamazaki, B. Cressiot, Q. Zhao, P. C. Whitford and M. Wanunu, Nanopore-based measurements of protein size, fluctuations, and conformational changes, *ACS Nano*, 2017, **11**, 5706–5716.

48 H. Wu, H. Liu, S. Tan, J. Yu, W. Zhao, L. Wang and Q. Liu, The estimation of field-dependent conductance change of nanopore by field-induced charge in the translocations of AuNPs-DNA conjugates, *J. Phys. Chem. C*, 2014, **118**, 26825–26835.

49 S. W. Kowalczyk, D. B. Wells, A. Aksimentiev and C. Dekker, Slowing down DNA translocation through a nanopore in lithium chloride, *Nano Lett.*, 2012, **12**, 1038–1044.

50 M. Wanunu, W. Morrison, Y. Rabin, A. Y. Grosberg and A. Meller, Electrostatic focusing of unlabelled DNA into nanoscale pores using a salt gradient, *Nat. Nanotechnol.*, 2010, **5**, 160.

51 P. Sherman, Rheology of disperse systems, *Industrial Rheology*, Academic Press Inc., London, 1970, pp. 97–183.

52 S. E. Henrickson, M. Misakian, B. Robertson and J. J. Kasianowicz, Driven DNA transport into an asymmetric nanometer-scale pore, *Phys. Rev. Lett.*, 2000, **85**, 3057.

53 B. Cressiot, A. Oukhaled, G. Patriarche, M. Pastoriza-Gallego, J.-M. Betton, L. c. Auvray, M. Muthukumar, L. Bacri and J. Pelta, Protein transport through a narrow solid-state nanopore at high voltage: experiments and theory, *ACS Nano*, 2012, **6**, 6236–6243.

54 A. Oukhaled, B. Cressiot, L. Bacri, M. Pastoriza-Gallego, J.-M. Betton, E. Bourhis, R. Jede, J. Gierak, L. Auvray and J. Pelta, Dynamics of completely unfolded and native proteins through solid-state nanopores as a function of electric driving force, *ACS Nano*, 2011, **5**, 3628–3638.

55 I. Gitlin, J. D. Carbeck and G. M. Whitesides, Why are proteins charged? Networks of charge–charge interactions in proteins measured by charge ladders and capillary electrophoresis, *Angew. Chem., Int. Ed.*, 2006, **45**, 3022–3060.

56 N. Grover, J. Naaman, S. Ben-Sasson and F. Doljanski, Electrical sizing of particles in suspensions, *Biophys. J.*, 1969, **9**, 1398–1414.

57 R. DeBlois and C. Bean, Counting and sizing of submicron particles by the resistive pulse technique, *Rev. Sci. Instrum.*, 1970, **41**, 909–916.

58 G. Di Muccio, A. E. Rossini, D. Di Marino, G. Zollo and M. Chinappi, Insights into protein sequencing with an α-Hemolysin nanopore by atomistic simulations, *Sci. Rep.*, 2019, **9**, 1–8.

59 J. Wilson, K. Sarthak, W. Si, L. Gao and A. Aksimentiev, Rapid and accurate determination of nanopore ionic current using a steric exclusion model, *ACS Sens.*, 2019, **4**, 634–644.